Supporting Information

Alkylthio side chain tuned the PM6 structure and elevated photovoltaic performance in ternary donor polymers

Pengzhi Guo,[a,b] Jinye He,[a] Junhong Liang,[a] Tiantian Wang,[a] Mingruo Li,[a] Jianhong Wei,[a] Wentao Miao,[a] Zezhou Liang,[c] Yuan Zhou,[a] Junfeng Tong,[b] Xunchang Wang,[d] Chenglong Wang[a] and Yangjun Xia*[b]*

[a] National Engineering Research Center for Technology and Equipment of Environmental Deposition, Solar Thermal Industry Research Institute of Gansu Province Lanzhou Jiaotong University, Lanzhou 730070, P. R. China.

[b] Organic Semiconductor Materials and Applied Technology Research Centre of Gansu Province, School of Materials Science and Engineering, Lanzhou Jiaotong University, Lanzhou, 730070, P. R. China.

[c] Key Laboratory for Physical Electronics and Devices of the Ministry of Education and Shaanxi Key Lab of Photonic Technique for Information, School of Electronics and Information Engineering, Xi'an Jiaotong University, Xi'an, 710049, P. R. China.

[d] Key Laboratory of Optoelectronic Chemical Materials and Devices (Ministry of Education), School of Optoelectronic Materials & Technology, Jianghan University, Wuhan 430056, P. R. China.

Corresponding Author:

E-mail: shxygpz@126.com (P.G.).

Xiayangjun2016@126.com (Y.X.)

Tel : +86-0931-495-6058 (P.G.).

1. Experimental section

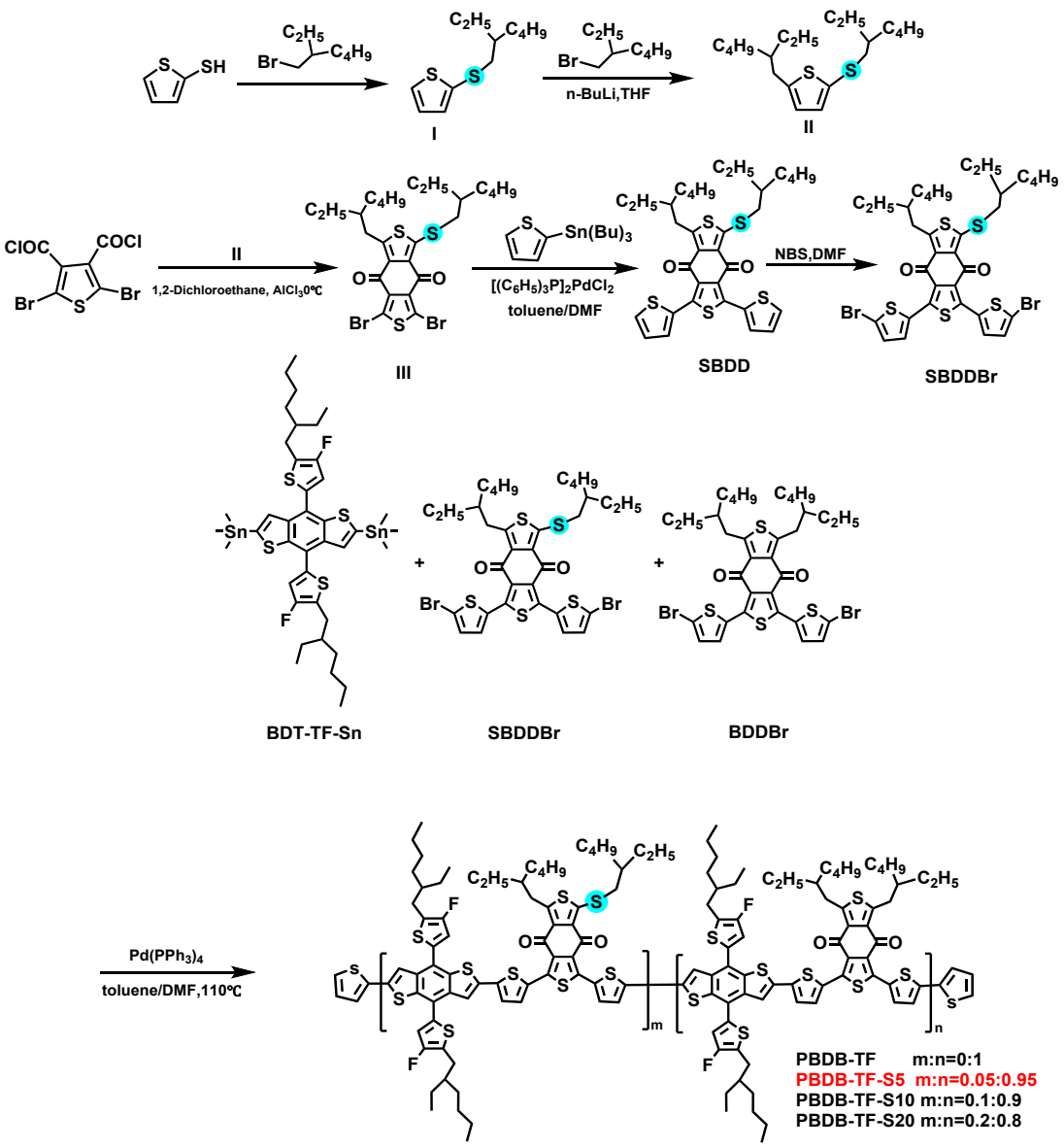

Scheme S1 Synthetic routes of the monomers and polymers.

1.1 Synthesis of monomers and polymers

All reagents were purchased from Energy Chemical, Aladdin, (Shanghai, China), Sigma-Aldrich Co., unless otherwise noted. And Tokyo Chemical Industry Co., and use as received. Toluene, tetrahydrofuran (THF) and *N,N*-dimethylformamide (DMF) were distilled according to common methods. Column chromatography was carried out with Merck silica gel (200–300 mesh). 2-bis(trimethyltin)-5,10-bis(4-fluoro-5-(2-ethylhexyl)thien-2-yl)benzo[1,2-b:4,5-b']di-thiophene (BDT-TF-Sn)[1], (BDDBr)[2], I, II, III,[3] and poly[(2,6-(4,8-bis(5-(2-ethylhexyl-3-fluoro)thien-2-yl)-benzo[1,2-b:4,5-b']dithiophene))-*alt*-(5,5-(1',3'-di-2-thienyl-5',7'-bis(2-

ethylhexyl)benzo[1',2'-c:4',5'-c']dithiophene-4,8-dione)]] (PBDB-TF)[4] were synthesized according to the procedure reported in the literature.

1.1.1 1,3-Bis(thien-2-yl)-5-(2-ethylhexyl)-7-(2-ethylhexylthio)-4*H*,8*H*-benzo[1,2-c:4,5-c′]-dithiophene-4,8-dione (SBDD)

Compound 1,3-dibromo-5-(2-ethylhexyl)-7-(2-ethylhexylthio)-4*H*,8*H*-benzo[1,2-c:4,5-c']-dithiophene-4,8-dione (III) (3.0 g, 4.7 mmol) and 2-trimethylstannylthiophene (3.5 g, 14.2 mmol) were dissolved in a mixture of 50 mL toluene and 5 mL DMF. Purge the mixture with N_2 for 20 minutes before adding $Pd(PPh_3)_2Cl_2$ (0.22 g, 0.235 mmol) to the flask. The reaction was carried out at 110 °C in N_2 for 8 h. The mixture was then cooled to room temperature and extracted with DCM. The yellow solid powder (2.1g, 71%) was purified by column chromatography with PE:DCM (5:2) as eluent. ^{1}H NMR (500 MHz, Chloroform-d) δ 7.76 (dd, *J* = 31.2, 3.7 Hz, 2H), 7.49 (dd, *J* = 9.8, 5.1 Hz, 2H), 7.12 (dd, *J* = 5.3, 3.8, 2.2 Hz, 2H), 3.32 (d, *J* = 7.0 Hz, 2H), 3.03 (d, *J* = 6.4 Hz, 2H), 1.77 (dd, *J* = 12.8, 6.4 Hz, 3H), 1.48 (dd, *J* = 12.0, 6.6 Hz, 4H), 1.32 (dd, *J* = 7.2, 3.7 Hz, 14H), 0.96–0.87 (m, 15H).

1.1.2 1,3-bis(5-bromothiophene-2-yl)-5-(2-ethylhexyl)-7-(2-ethylhexylthio)-4H,8H-benzo[1,2-c:4,5-c']dithiophene-4,8-dione (SBDDBr)

Compound SBDD (2g, 3.12mmol) was dissolved in a double-mouth flask with a mixed solution of DMF and $CHCl_3$. NBS (1.39 g, 7.8 mmol) was poured into the bottle, stirred at room temperature, and detected by point plate. After the reaction was completed, it was washed with a large amount of water, extracted, dried and concentrated. The yellow solid (2.07g, 83%) was purified by silica gel column using analytically pure PE:DCM (5:2) as eluent. ^{1}H NMR (500 MHz, Chloroform-d) δ 7.45 (dd, *J* = 11.1, 4.0 Hz, 2H), 7.06 (t, *J* = 4.0 Hz, 2H), 3.31 (qd, *J* = 15.2, 7.0 Hz, 2H), 3.04 (d, *J* = 7.6 Hz, 2H), 1.85-1.69 (m, 3H), 1.54-1.26 (m, 19H), 1.00-0.87 (m, 14H). ^{13}C NMR (126 MHz, Chloroform-d) δ 177.06, 175.84, 153.31, 151.28, 142.00, 141.02, 134.62, 134.41, 132.72, 131.96, 131.36, 130.46, 130.40, 129.85, 129.75, 118.19, 117.98, 41.39, 38.86, 33.63, 32.77, 32.67, 28.82, 25.97, 25.81, 23.05, 22.96, 14.23, 14.12, 10.88, 10.75.

1.2 Syntheses of PBDB-TF, PBDB-TF-S5, PBDB-TF-S10 and PBDB-TF-S20

1.2.1 Syntheses of PBDB-TF[4]

Purified di-tin monomer BDT-TF-Sn (141 mg, 0.15 mmol), di-bromo monomer BDDBr (114.7 mg, 0.15 mmol) were weighed and put into a 25 mL double-necked flask, and 8 mL of dried toluene was added. The argon was purged with a long needle for 20 min to replace the oxygen in the reaction system to create an anhydrous and anaerobic environment. The (0)-valent palladium catalyst $Pd(PPh_3)_4$ (10 mg) was quickly added to the reaction system. Continue to purge with argon for 10–15 min. The reaction was heated to reflux for 24 h. Toluene dissolved with BDT-TF-

Sn (8 mg) and $Pd(PPh_3)_4$ (5 mg) was injected into the reaction system with a syringe to eliminate bromine at both ends of the polymer. After 4h of reaction, 0.2 mL of 2-bromothiophene was added to eliminate tin at both ends. The reaction was completed after 4 h. Drop the reaction into a 150 mL beaker and filter the solids. Then, the crude product was wrapped in filter paper and put into Soxhlet extractor, washed with methanol, acetone, n-hexane, dichloromethane and chloroform in turn (79%).

1.2.2 Syntheses of PBDB-TF-S5

Purified di-tin monomer BDT-TF-Sn (141 mg, 0.15 mmol), di-bromo monomer SBDDBr (6 mg, 0.0075 mmol) and another di-bromo monomer BDDBr (109 mg, 0.1425 mmol) were weighed and put into a 25 mL double-necked flask, and 8 mL of dried toluene was added. The argon was purged with a long needle for 20 min to replace the oxygen in the reaction system to create an anhydrous and anaerobic environment. The $Pd(PPh_3)_4$ (10 mg) was quickly added to the reaction system. Continue to purge with argon for 10-15 min. The reaction was heated to reflux for 24 h. Toluene dissolved with BDT-TF-Sn (8 mg) and $Pd(PPh_3)_4$ (5 mg) was injected into the reaction system with a syringe to eliminate bromine at both ends of the polymer. After 4h of reaction, 0.2 mL of 2-bromothiophene was added to eliminate tin at both ends. The reaction was completed after 4 h. Drop the reaction into a 150 mL beaker and filter the solids. Then, the crude product was wrapped in a re-filter paper and placed in a Soxhlet extractor. It was washed with methanol, acetone, n-hexane, dichloromethane and chloroform in turn, and the part dissolved in chloroform was collected. After concentration, it was dripped into methanol again, filtered and dried to obtain a solid (76%).

1.2.3 Syntheses of PBDB-TF-S10

PBDB-TF-S10 was the same as the above synthesis method, but the double tin monomer was replaced with BDT-TF-Sn (141 mg, 0.15 mmol), double bromine monomer SBDDBr (11.98 mg, 0.015 mmol) and BDDBr (103.4 mg, 0.135 mmol) in toluene solution, and $Pd(PPh_3)_4$ was used to catalyze Stille coupling to synthesize PBDB-TF-S10 (83%).

1.2.4 Syntheses of PBDB-TF-S20

PBDB-TF-S20 was the same as the above synthesis method, but the double tin monomer was replaced by BDT-TF-Sn (141 mg, 0.15 mmol), double bromine monomer SBDDBr (24 mg, 0.03 mmol) and BDDBr (92 mg, 0.12 mmol) in toluene solution, and $Pd(PPh_3)_4$ was used to catalyze Stille coupling to synthesize PBDB-TF-S20 (74%).

1.3 Measurement and characterization

^{1}H NMR spectra was measured on a Bruker 500 MHz AVANCE NEO (Rheinstetten, Germany) spectrometer, with tetramethylsilane (TMS) as the internal reference. Chemical shifts (δ) were recorded in units of ppm and their splitting patterns were designed as *s* (singlet), *d* (doublet), *t* (triplet), *m* (multiplet), and *br* (broaden). Note that chloroform-d ($CDCl_3$) residual peak was taken as internal reference at 7.26 ppm for ^{1}H NMR. TGA curves were collected on a TGA 2050 instruments (New Castle, DE, USA) at the heating rate of 10 ℃·min^{-1} and under a N_2 flow rate (20 mL·min^{-1}). UV-Vis absorption measurement was performed on a UV-1800 spectrophotometer (Shimadzu, Kyoto, Japan). Thin film X-ray diffraction (XRD) was recorded on a PANalytical X'Pert PRO diffractometer equipped with a rotating anode (Cu *K*α radiation, λ= 1.54056 Å). The electrochemical properties of films were measured on a CHI600D electro-chemical instrument (Chenhua, Shanghai, China) in anhydrous CH_3CN at a scan rate of 100 mV·s^{-1} under N_2. Tetra(n-butyl)ammonium hexafluorophosphate (Bu_4NPF_6) (0.1 mol·L^{-1}) was utilized as the electrolyte. A three-electrode cell was used in all experimental, wherein glassy carbon electrode coated by polymer film, platinum wire and Ag/$AgNO_3$ (0.01 M of $AgNO_3$ in CH_3CN) electrode were used as the working, counter and reference electrode, respectively. The potential of Ag/$AgNO_3$ reference electrode was calibrated by the ferrocene/ferrocenium couple (Fc/Fc^+), whose energy level was 4.80 eV. Note that polymer's thin films were obtained by dropcasting 1 μL studied material chlorobenzene solution with the concentration of 1 mg·mL^{-1} onto the glass carbon electrode, and then dried in the air. The contact angle was measured with an optical contact angle measuring and contour analysis systems (Dataphysics OCA 25). Atomic force microscopy (AFM) images were acquired on an MFP-3D-SA (Asylum Research, Santa Barbara, CA, USA) in a tapping mode.

1.4 Fabrication of OSCs and mobility characterization

The photovoltaic device preparation process is as follows：

(1) Cleaning and pretreatment of ITO substrate: The back of ITO glass was numbered, and ultrasonic cleaning machine was used to wash twice with surfactant solution, acetone, ultrapure water and isopropanol, 10 min each time. Finally, it was stored in isopropanol solution.

(2) Preparation of hole transport layer：After drying under nitrogen flow, the substrates were treated with oxygen plasma for 10 min, then a thin layer of poly(3,4-ethylenedioxythiophene):poly(styrene-sulfonate) (PEDOT:PSS, ca. 40 nm, Clevios PVP Al4083) was spin-coated onto the ITO substrates and annealed at 150 ℃ for 20 min.

(3) Preparation of active layer：After that the substrates were transferred into a nitrogen-filled glove box and the active layer was prepared. The active layer, with a thickness in the 100–120 nm range, was deposited on top of the PEDOT:PSS layer by spin-casting from chloroform solution

containing the studied materials.

(4) Preparation of electron transport layer: PDINN (1 mg/mL^{-1} in methanol) was spin-coated on the active layer at a speed of 3000 rpm/min.

(5) Preparation of electrode: The Al layer (~100 nm) as the cathode was thermally evaporated at a vacuum pressure of 10^{-4} Pa. The thickness values of the evaporated Al were monitored by a quartz crystal thickness/ratio monitor (SI-TM206, Shenyang Sciens Co.).

The PCEs of the resulting PSCs were measured under 1 sun, AM 1.5G (Air mass 1.5 global) condition using a solar simulator (XES70S1, San-EI Electric Co.) with irradiation of 100 mW·cm^{-2}. The current density-voltage (*J-V*) characteristics were recorded with a Keithley 2400 source-measurement unit. The spectral responses of the devices were measured with a commercial external quantum efficiency (EQE)/incident photon to charge carrier efficiency (IPCE) setup (7-SCSpecIII, Beijing 7-star Opt. In. Co.) equipped with a standard Si diode.

The hole-only and electron-only devices were prepared with a diode configuration of ITO/PEDOT:PSS/Active layer/MoO_3/Ag or ITO/ZnO/Active layer/PDINN/Ag, respectively. The device characteristics were extracted by modeling the dark current under an applied forward bias. The hole and electron mobilities of the active layers were extracted by fitting the current-voltage curves using the Mott-Gurney relationships (space-charge-limited current, SCLC).[5] The field dependent SCLC behavior can be expressed as: $J = \frac{9}{8}\varepsilon_0\varepsilon_r\mu\frac{V^2}{L^3}$.Where J stands for the current density, ε_0 is the permittivity of free space (8.85×10^{-12} F·m^{-1}), ε_r is the relative permittivity of the transport medium (assumed to be 3, which is a typical value for CPs), μ is the zero-field mobility of hole or electron, L is the thickness of the active layer, and effective voltage $V = (V_{appl} - V_{bi})$, where V_{appl} is the applied voltage to the device and V_{bi} is the built-in voltage. By linearly fitting $J^{1/2}$ with V, the mobilities were extracted from the slope and L: $\mu = \frac{slope^2 \times 8L^3}{9\varepsilon_0\varepsilon_r}$. For the hole-only devices, V_{bi} is 0 V, while V_{bi} = 0.7 V in the electron-only devices.

1.5 Device photostability characterizations

The photostability data of the devices was measured by using Maximum Power Point (MPP) tracking mode (YH-VMPP-IV-16). The decay curves of these encapsulated devices were measured under continuous LED light source (380-810 nm, one solar intensity) in N_2 atmosphere (the average humidity was 20%, the average tested temperature was 25℃).

1.6 Surface energy calculation[6, 7]

The surface tension (γ) can be evaluated using the Wu model, via Equations (1), (2), and (3), on

the basis of the measured contact angles (θ) information.

$$\gamma_{water}(1+cos\theta_{water}) = \frac{4\gamma_{water}^{d}\gamma^{d}}{\gamma_{water}^{d}+\gamma^{d}} + \frac{4\gamma_{water}^{p}\gamma^{p}}{\gamma_{water}^{p}+\gamma^{p}} \quad (1)$$

$$\gamma_{EG}(1+cos\theta_{EG}) = \frac{4\gamma_{EG}^{d}\gamma^{d}}{\gamma_{EG}^{d}+\gamma^{d}} + \frac{4\gamma_{EG}^{p}\gamma^{p}}{\gamma_{EG}^{p}+\gamma^{p}} \quad (2)$$

$$\gamma = \gamma^{d} + \gamma^{p} \quad (3)$$

Where, γ is the surface energy of the studied semiconductor; γ^d and γ^p are the dispersion and polar components of γ; γ_i is the total surface energy of the i material (i = water or ethylene glycol); γ_i^d and γ_i^p are the dispersion and polar components of γ_i; and θ is the droplet contact angle (water or ethylene glycol) on the semiconductor film. Flory–Huggins interaction parameter $\chi^{donor-acceptor}$, which is a parameter to evaluate the interaction between polymeric donors and acceptor Y6, based on this, the miscibility of the two components can be objectively judged. The smaller the difference of surface energy between donor and acceptor, the lower the value of $\chi^{donor-acceptor}$ and the better the miscibility.

1.7 Femtosecond time-resolved Transient Absorption (fs-TA) Measurements[8]

Fs-TA spectroscopy was performed to measure the temporal evolution of the absorption changes in the excited states, through which the carrier dynamics in femtosecond to nanosecond regime could be revealed. The laser beam is supplied by amplified Ti: sapphire laser source (800 nm, Coherent) that provides 100 fs pulses with a repetition rate of 1 kHz. The output was split into two beams, the stronger one of which was frequency doubled to generate a 400 nm pump light, and the other one was focused into a sapphire plate to generate a broadband supercontinuum probe light. Using an optical chopper, the repetition rate of the pump pulses was adjusted to 500 Hz, and was focused on the sample with the probe pulse (white light). The TA spectra were obtained by comparing the probe light spectra with and without pump light excitation. The photo-induced absorption change as a function of wavelength was described using optical density (absorbance) changes ($\Delta OD(\lambda)$). By adjusting the delay time between the pump and probe pulses, a 3D transient spectral image ($\Delta OD(\lambda,)$) was formed.

1.8 Energy loss Calculation

The total energy loss (E_{loss}) can be attributed to three components following the equations

below:

$$E_{loss} = E_g - qV_{oc} \quad (4)$$

$$= (E_g - qV_{oc}^{SQ}) + (qV_{oc}^{SQ} - qV_{oc}^{rad}) + (qV_{oc}^{rad} - qV_{oc})$$

$$= (E_g - qV_{oc}^{SQ}) + q\Delta V_{oc}^{rad,below\ gap} + q\Delta V_{oc}^{non-rad}$$

$$= \Delta E_1 + \Delta E_2 + \Delta E_3$$

where E_g is the bandgap, q is the elementary charge, V_{oc}^{SQ} is the maximum voltage based on the Shockley-Queisser limit (SQ limit), V_{oc}^{rad} is the open-circuit voltage when there is only radiative recombination, $\Delta V_{oc}^{rad,below\ gap}$ is the voltage loss of radiative recombination from the absorption below the bandgap and $\Delta V_{oc}^{non-rad}$ is the voltage loss of non-radiative recombination. ΔE_1 is due to radiative recombination from absorption above the bandgap, ΔE_2 is due to radiative recombination from absorption below the bandgap, and ΔE_3 is due to non-radiative recombination. The third component, the non-radiative loss, could be directly calculated by the following relation:

$$\Delta E_3 = qV_{oc}^{rad} - qV_{OC} = -kTIn(EQE_{EL}) \quad (5)$$

where k is the Boltzmann constant, T is temperature and EQE_{EL} is the radiative quantum efficiency of the OSCs when charge carriers are injected into the device in the dark.

$$EQE_{EL} = \gamma\chi\Phi_{PL}\eta_{out} \quad (6)$$

Where EQE_{EL} is the electroluminescence quantum efficiency of solar cells via injecting charge carriers into the device under dark, γ is the charge balance factor (typically stipulated to be 1), χ is the fraction of recombination events due to the radiative decay (the spin-singlet configuration in excitons), Φ_{PL} is the photoluminescence quantum efficiency (equivalent to the luminescence yield of spin-singlet excitons) and η_{out} is the photon out-coupling efficiency (generally evaluated to be 0.3).

2. Supplementary figures and tables

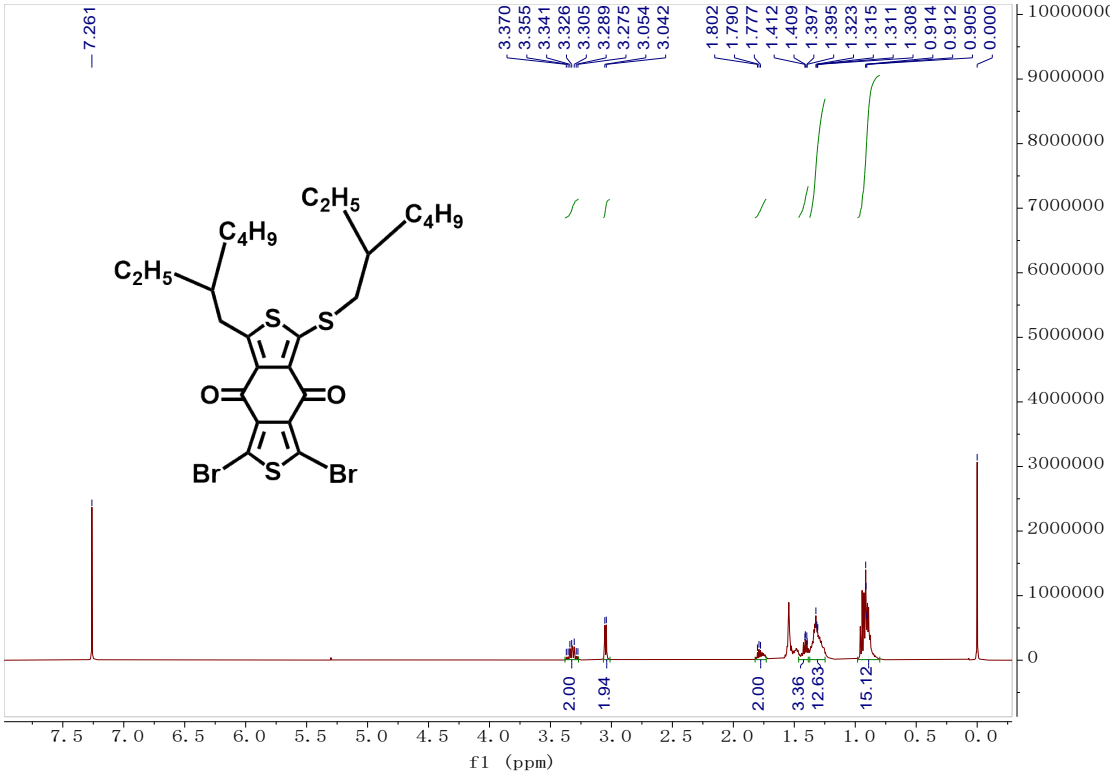

Fig. S1. ^{1}H NMR spectrum of III in $CDCl_3$.

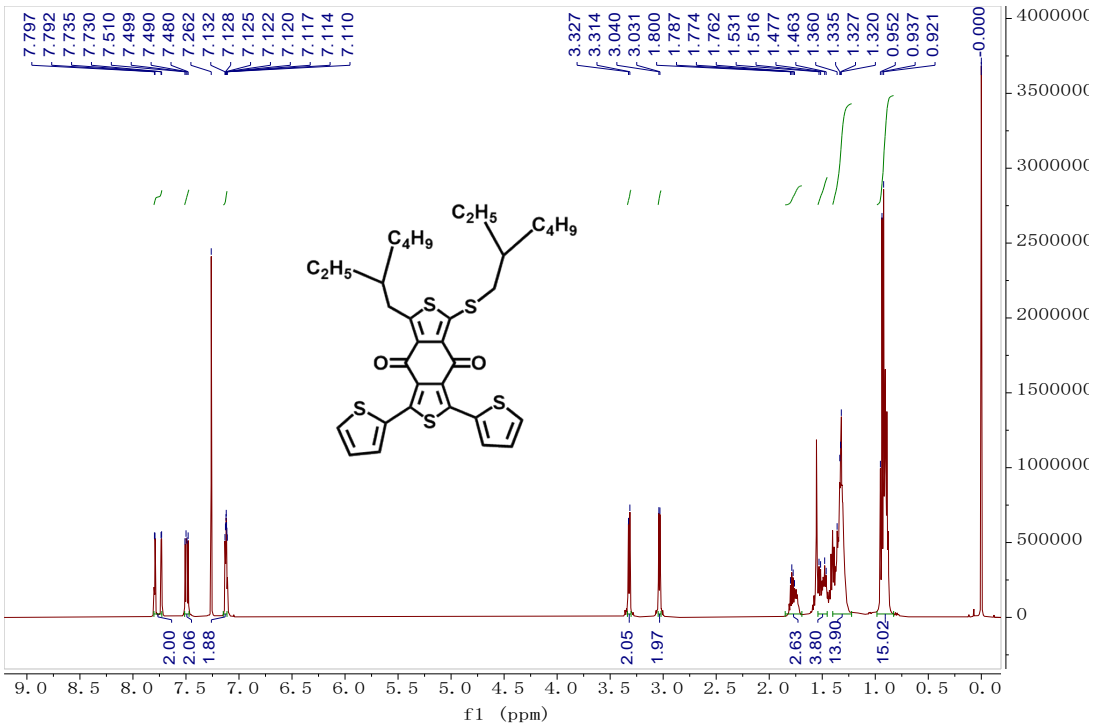

Fig. S2. ^{1}H NMR spectrum of SBDD in $CDCl_3$.

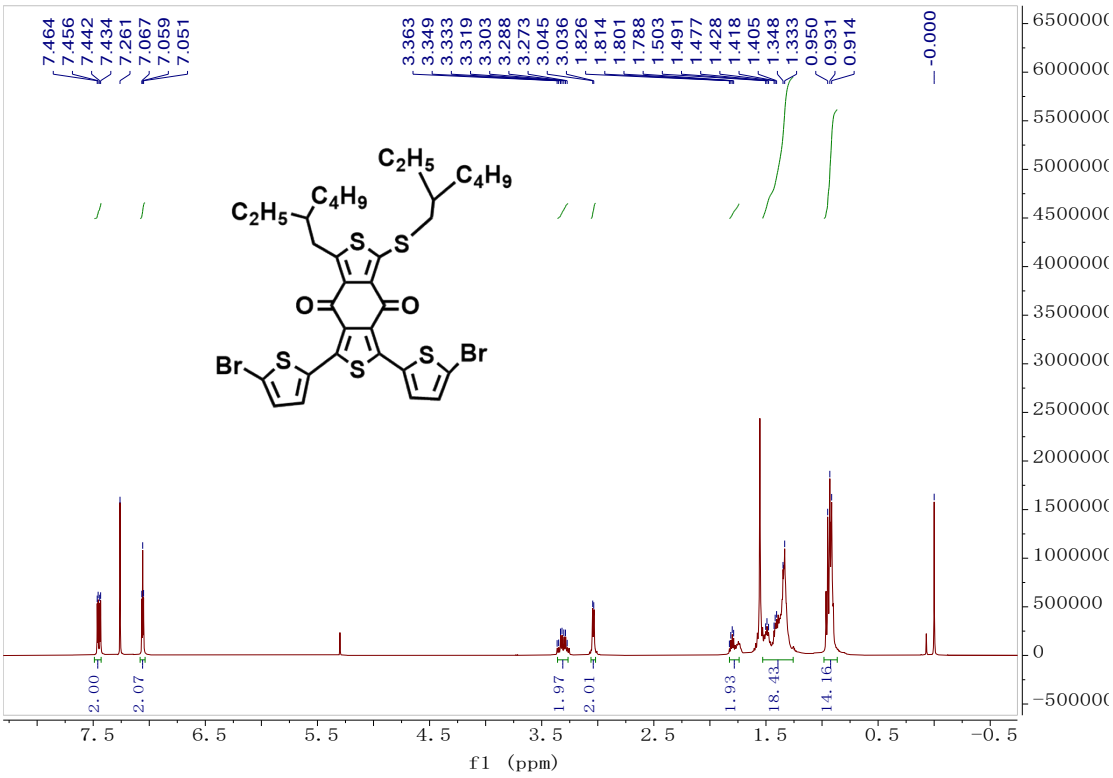

Fig. S3. ^{1}H NMR spectrum of SBDDBr in $CDCl_3$.

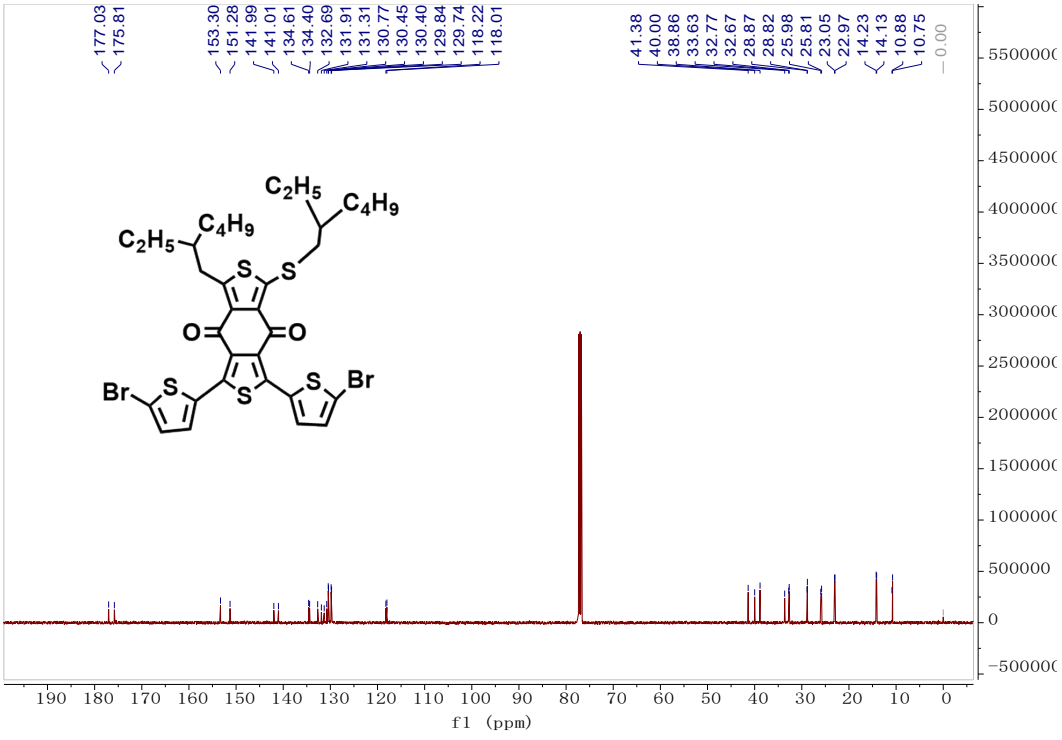

Fig. S4. ^{13}C NMR spectrum of SBDDBr in $CDCl_3$.

Table S1 Yield, GPC, TG data of polymers.

Polymer	T_d (°C)	M_n (kDa)	M_w (kDa)	PDI	Yield (%)
PBDB-TF	430	20.2	40.4	2.0	79
PBDB-TF-S5	429	20.6	35.0	1.7	76
PBDB-TF-S10	420	21.3	44.7	2.1	83
PBDB-TF-S20	404	19.7	37.43	1.9	74

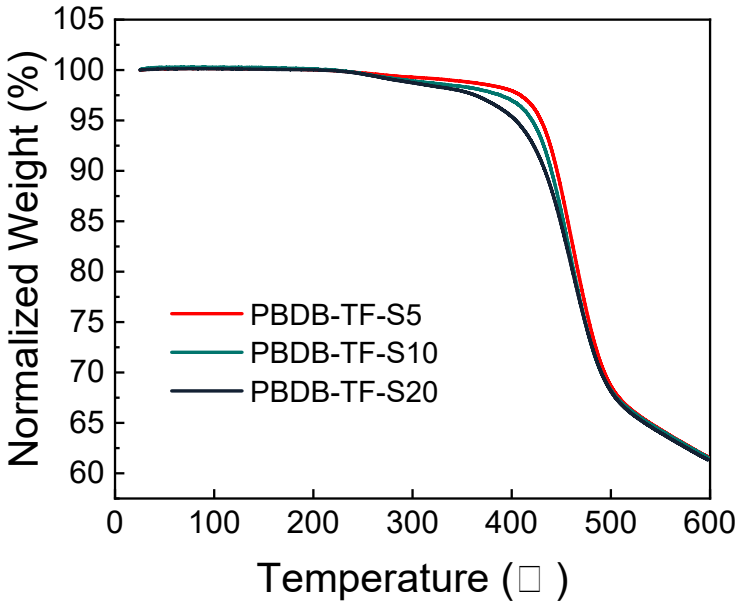

Fig. S5. TG curves of PBDB-TF-S5, PBDB-TF-S10 and PBDB-TF-S20.

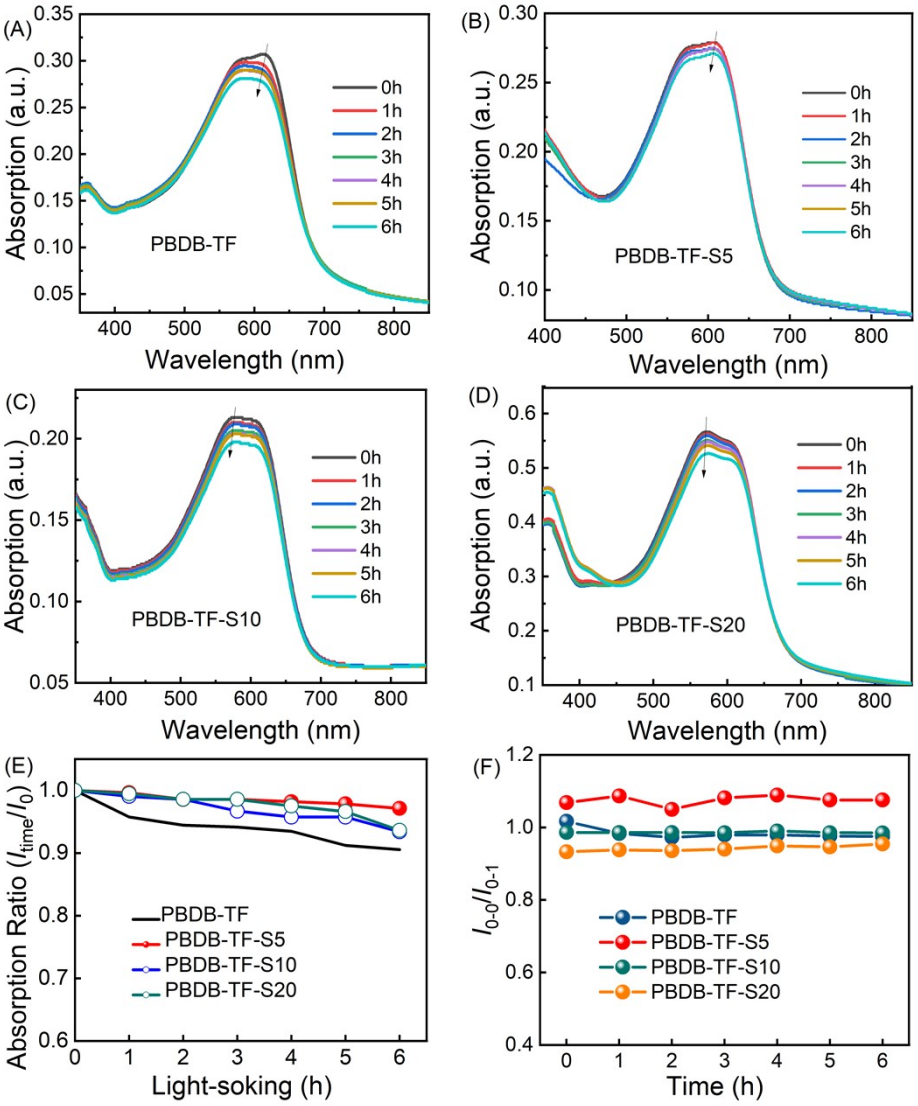

Fig. S6. Absorption spectra of polymer films under different exposure time.

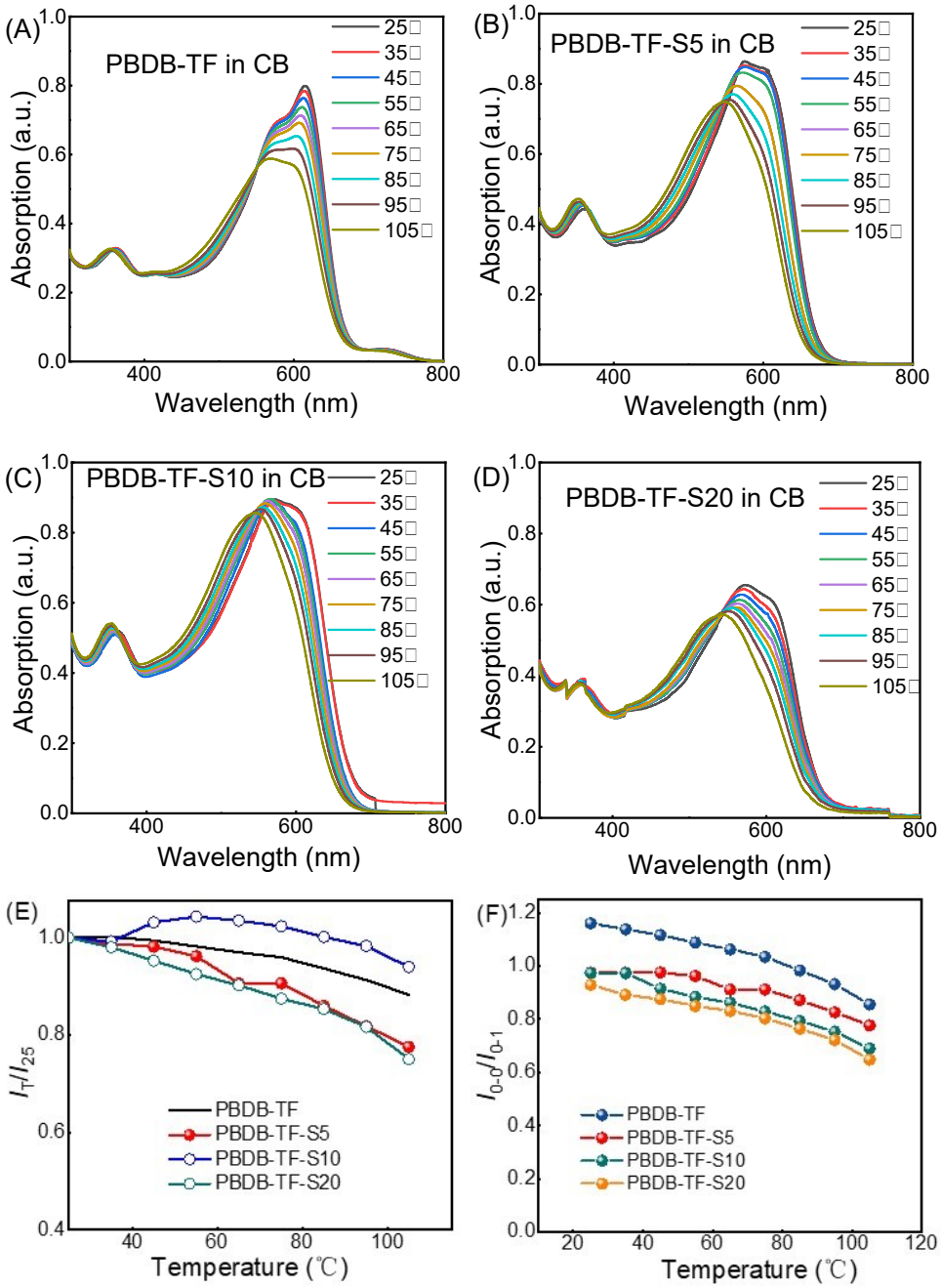

Fig. S7. Temperature-dependent UV-vis spectra for polymers in CB.

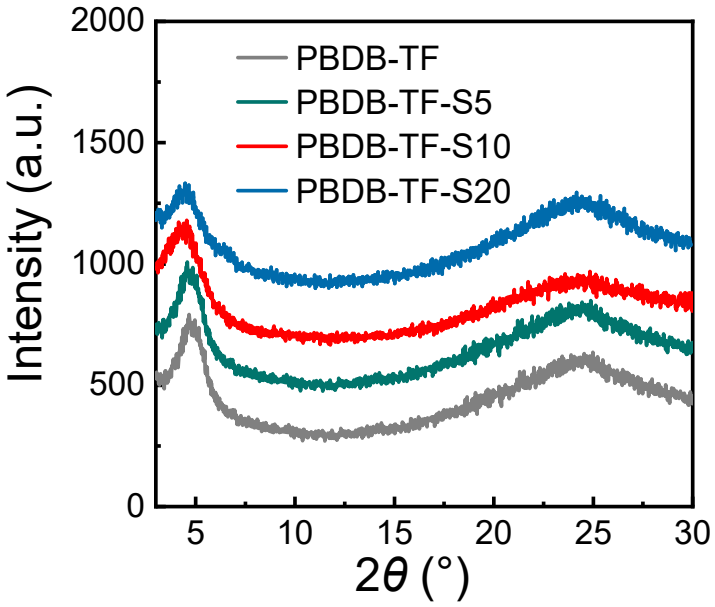

Fig.S8. XRD diffraction pattern of polymer in thin film state.

Table S2. Detailed XRD parameters of polymers.

Polymer	$2\theta_1$ (°)	$2\theta_2$ (°)	d_L (Å)	d_π (Å)
PBDB-TF	4.68	24.64	18.85	3.58
PBDB-TF-S5	4.58	24.42	19.26	3.60
PBDB-TF-S10	4.56	24.40	19.34	3.61
PBDB-TF-S20	4.48	24.14	19.69	3.65

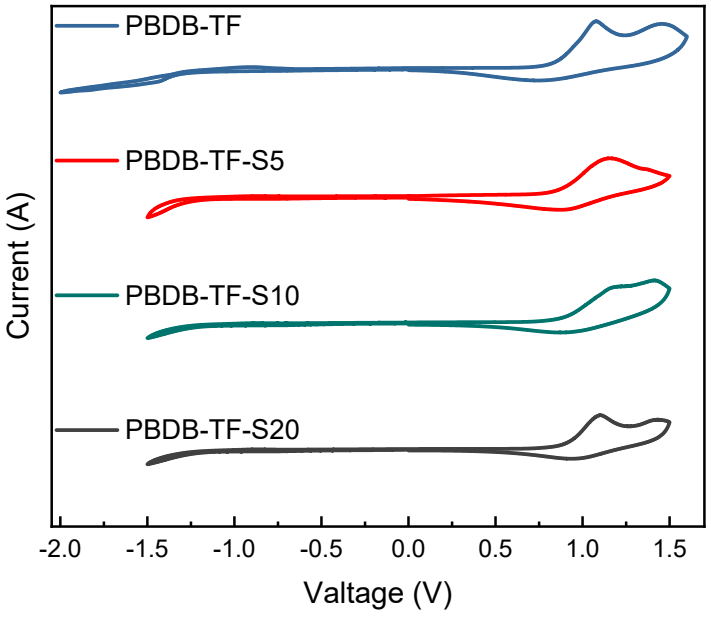

Fig. S9. CV curves for polymers donors.

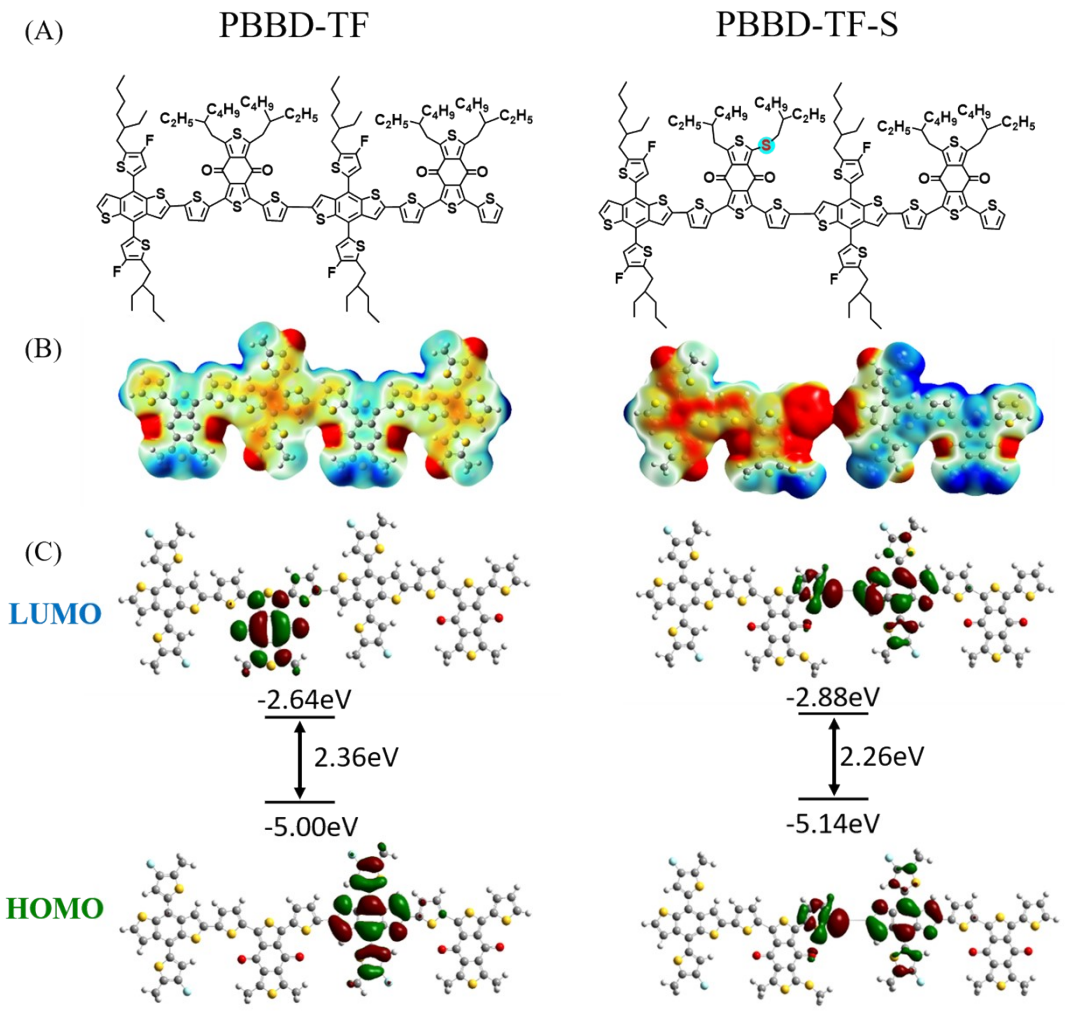

Fig. S10. (A) Molecular structures of the polymers. (B) ESP distribution (C) Frontier orbital energy of the model structures.

Table S3. Photovoltaic device parameters under different D/A radio.

Active layer	D/A radio	V_{OC} (V)	J_{SC} (mA·cm^{-2})	FF (%)	PCE (%)
PBDB-TF-S5:Y6	1:1.0	0.864	15.05	66.25	8.02
	1:1.2	0.874	22.86	49.69	9.92
	1:1.5	0.877	22.06	58.13	11.25
	1:1.8	0.869	22.68	55.62	10.97
PBDB-TF-S10:Y6	1:1.0	0.895	16.77	59.01	8.86
	1:1.2	0.890	18.01	59.84	9.60
	1:1.5	0.891	18.45	59.34	9.76
	1:1.8	0.887	18.27	59.37	8.55
PBDB-TF-S20:Y6	1:1.0	0.924	13.79	45.16	5.76
	1:1.2	0.920	17.04	53.07	8.32
	1:1.5	0.910	21.48	54.57	10.67
	1:1.8	0.906	21.26	53.83	10.37

Table S4. Photovoltaic parameters of devices with different thermal annealing (TA).

Active layer	Annealing (℃)	V_{OC} (V)	J_{SC} (mA·cm^{-2})	FF (%)	PCE (%)
PBDB-TF-S5:Y6=1:1.5	0	0.877	22.06	58.13	11.25
	90	0.862	20.30	67.60	11.83
	100	0.869	20.10	70.35	12.30
	110	0.867	22.30	65.01	12.58
	120	0.854	22.48	64.46	12.38
PBDB-TF-S10:Y6=1:1.5	0	0.891	18.45	59.34	9.76
	90	0.877	17.45	65.83	10.04
	100	0.867	18.05	64.12	10.09
	110	0.868	18.76	62.13	10.12
	120	0.862	19.24	59.8	9.92
PBDB-TF-S20:Y6=1:1.5	0	0.910	21.48	54.57	10.67
	90	0.896	23.23	53.18	11.08
	100	0.884	23.30	54.78	11.28
	110	0.897	23.35	58.84	11.91
	120	0.873	23.46	55.22	11.31

Table S5. Photovoltaic parameters of devices using different additives.

Active layer	Additive (CN%)	V_{OC} (V)	J_{SC} (mA·cm^{-2})	FF (%)	PCE (%)
PBDB-TF-S5:Y6=1:1.5	0.0	0.867	22.30	65.01	12.58
	0.5	0.865	25.34	72.10	15.80
	1.0	0.861	25.68	74.45	16.46
	1.5	0.866	24.95	53.84	11.59
	2.0	0.863	23.70	51.18	10.47
PBDB-TF-10:Y6=1:1.5	0.0	0.868	18.76	62.13	10.12
	0.5	0.873	23.69	53.98	11.17
	1.0	0.867	24.43	53.19	11.28
	1.5	0.863	24.19	52.23	10.93
	2.0	0.858	18.41	62.03	9.81
PBDB-TF-20:Y6=1:1.5	0.0	0.897	23.35	58.84	11.91
	0.5	0.897	22.71	55.01	11.21
	1.0	0.893	23.61	59.23	12.49
	1.5	0.890	22.80	54.44	11.05
	2.0	0.898	14.76	55.41	7.35

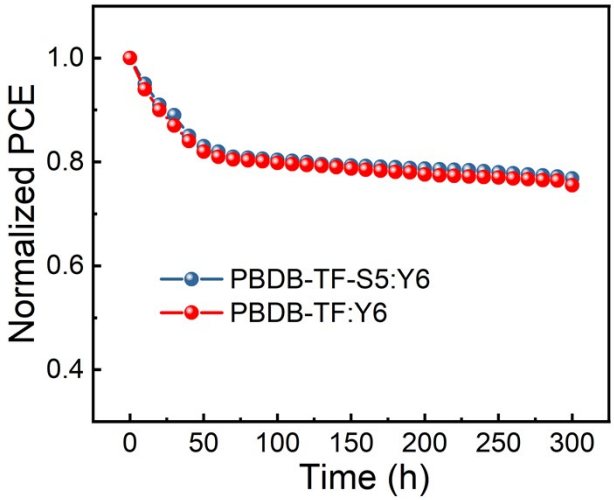

Fig.S11. Normalized PCE of PBDB-TF:Y6 and PBDB-TF-S5:Y6-based devices in the course of 300 h of LED light exposure.

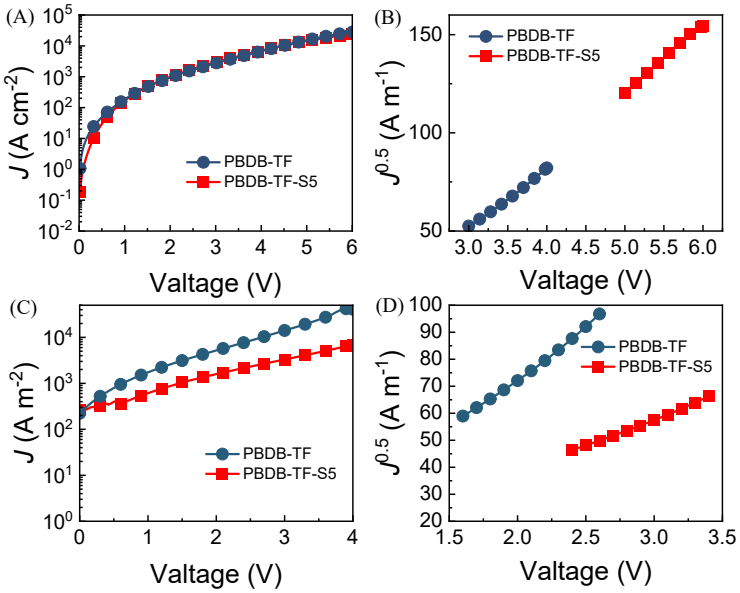

Fig. S12. The *J*-*V* (A, C) and $J^{1/2}$-*V* (B, D) curves of PBDB-TF and PBDB-TF-S5:Y6 electron transport devices and hole transport devices are given.

Table S6. Electron mobility of PBDB-TF and PBDB-TF-S5-based devices.

Active layer	Rations (w:w)	Slope	μ_h ($cm^2\ V^{-1}\ S^{-1}$)	μ_e ($cm^2\ V^{-1}\ S^{-1}$)	μ_h/μ_e
PBDB-TF:Y6	1:1.2	30.6	2.93×10^{-4}	3.43×10^{-4}	0.85
PBDB-TF-S5:Y6	1:1.5	30.4	3.97×10^{-4}	3.50×10^{-4}	1.13

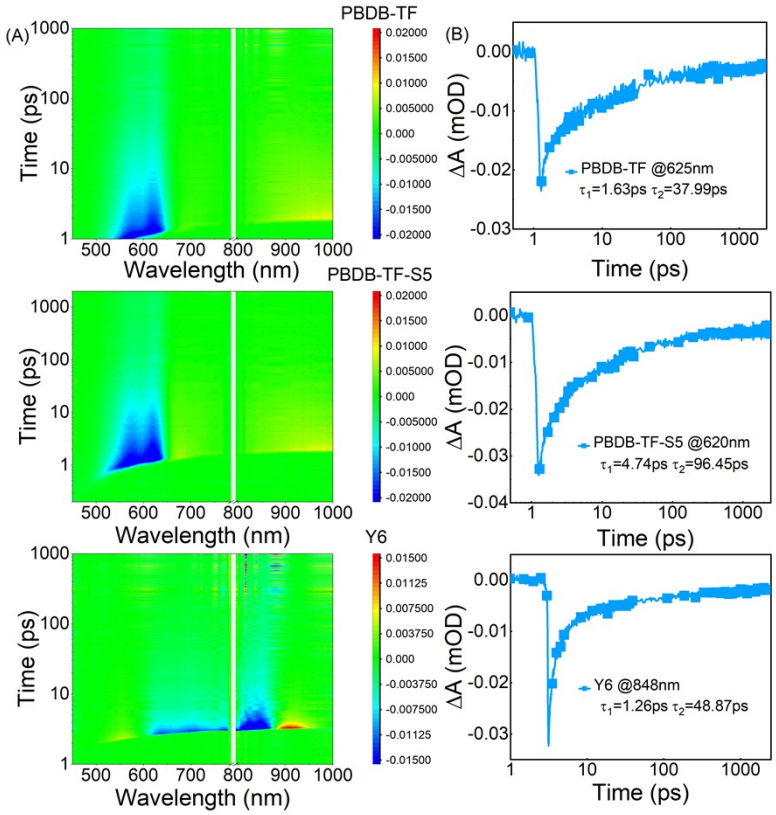

Fig. S13. TA spectra of (A)PBDB-TF pure film, PBDB-TF-S5 pure film and Y6 pure film, and B dynamics of PBDB-TF,PBDB-TF-S5, and Y6 pure films.

Table S7. GIWAXS data of the PBDB-TF:Y6 and PBDB-TF-S5:Y6 blend films.

Film	（010） diffraction peak				（100） diffraction peak			
	Q [Å^{-1}]	D [Å]	FWHM [Å^{-1}]	CCL [Å]	Q [Å^{-1}]	D [Å]	FWHM [Å^{-1}]	CCL [Å]
PBDB-TF:Y6	1.71	3.785	0.367	18.61	0.296	21.23	0.078	91.30
PBDB-TF-S5:Y6	1.66	3.674	0.314	15.92	0.294	21.37	0.064	74.91

Obtained using the equation of $D = 2\pi/Q$, in which Q is the corresponding x-coordinate of the diffraction peak. CCL is calculated using the equation: $CCL = 2\pi K/w$, in which w is the full-width-at-half maximum (FWHM) and K is a form factor ($K = 0.9$ here).

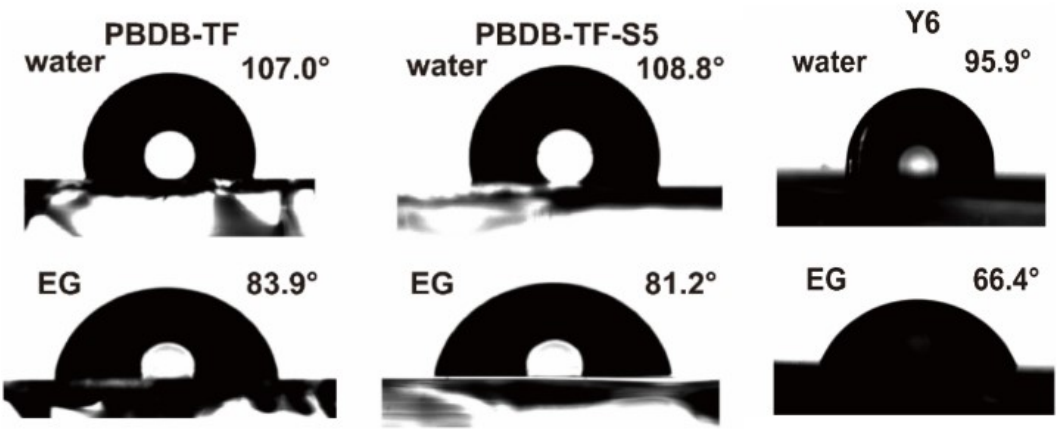

Fig. S14. The contact angle images of pure films PBDB-TF, PBDB-TF-S5 and Y6.

Table S8. Surface tension and interaction parameters of donor and acceptor.

Polymer	θ_{water} (°)	θ_{EG} (°)	γ^{total} (mN m^{-1})	χ
PBDB-TF	107.0	83.9	22.16	0.89
PBDB-TF-S5	108.8	81.2	22.39	0.84
Y6	95.9	66.4	31.93	-

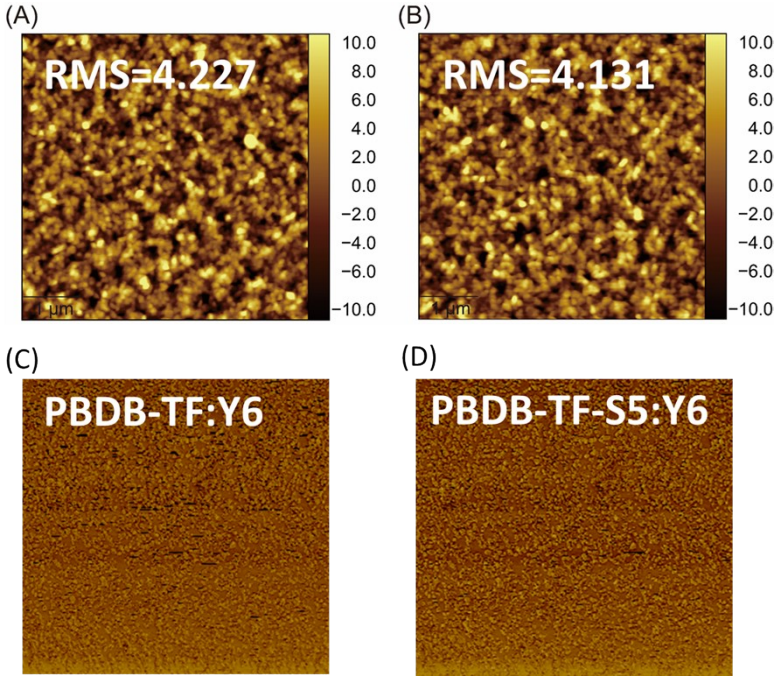

Fig. S15. AFM height images PBDB-TF:Y6 (A), PBDB-TF-S5:Y6 (B) and AFM phase images PBDB-TF:Y6 (C), PBDB-TF-S5:Y6 (D)

References

1. M. Zhang, X. Guo, S. Zhang and J. Hou, *Adv Mater.*, 2014, **26**, 1118-1123.
2. D. Qian, L. Ye, M. Zhang, Y. Liang, L. Li, Y. Huang, X. Guo, S. Zhang, Z. a. Tan and J. Hou, *Macromolecules*, 2012, **45**, 9611-9617.
3. K. Park, C. Sun, S.-Y. Jang, C. Wang, J. Li, Q. Zhao, H. Kang, K. Lee, S.-K. Kwon and Y.-H. Kim, *Dyes Pigm.*, 2020, **182**, 108601.
4. M. Zhang, X. Guo, W. Ma, H. Ade and J. Hou, *Adv Mater.,* 2015, **27**, 4655-4660.
5. X. Guo, N. Zhou, S. J. Lou, J. Smith, D. B. Tice, J. W. Hennek, R. P. Ortiz, J. T. L. Navarrete, S. Li, J. Strzalka, L. X. Chen, R. P. H. Chang, A. Facchetti and T. J. Marks, *Nat. Photonics*, 2013, **7**, 825-833.
6. J. Comyn, *Int. J. Adhes. Adhes.*, 1992, **12**, 145-149.
7. J. Tong, X. Jiang, H. Li, L. An, C. Yang, Y. Huang, P. Guo, Z. Liang, C. Yang, J. Li and Y. Xia, *Opt. Mater.*, 2021, **121**, 111593.
8. L. Yan, Z. Liang, J. Si, P. Gong, Y. Wang, X. Liu, J. Tong, J. Li and X. Hou, *ACS Appl. Mater. Interfaces*, 2022, **14**, 6945-6957.